



PERGAMON

Vacuum 59 (2000) 185–193

VACUUM

SURFACE ENGINEERING, SURFACE INSTRUMENTATION
& VACUUM TECHNOLOGY

www.elsevier.nl/locate/vacuum

Development of composite thermal barrier coatings with anisotropic microstructure

S. Sharafat^a, A. Kobayashi^{b,*}, V. Ogden^a, N.M. Ghoniem^a

^aMechanical & Aerospace Engineering Department, University of California, Los Angeles, CA 90095-1597, USA

^bJoining and Welding Research Institute, Osaka University, 11-1 Mihogaoka, Ibaraki, Osaka 567-0047, Japan

Abstract

A novel ZrO_2 - Al_2O_3 thermal barrier composite coating was produced using a gas-tunnel-type plasma spraying torch. To enhance visualization of the microstructure features, image enhancement techniques were used during the microphotograph digitization processes. The unique microstructure features of this composite coating include a relatively even distribution of embedded thin ZrO_2 splats in a Al_2O_3 matrix, parallel alignment of the ZrO_2 splats relative to the substrate surface, absence of porosity between the ZrO_2 splats and the Al_2O_3 matrix, etc. This anisotropic composite coating combined with the large difference in thermal conductivity between ZrO_2 and Al_2O_3 will alter the thermal behavior of the coating. © 2000 Elsevier Science Ltd. All rights reserved.

Keywords: Plasma spray; Composite ceramic coatings; Alumina; Zirconia; Anisotropic properties; Thermal barrier coating (TBC)

1. Introduction

The success of thermal barrier coatings (TBC) in high-temperature turbine blade applications has led to the recognition that TBC-coated superalloys offer the most viable materials solution to both near-and longer-term challenges posed by engines [1]. For example, diesel engine TBC research has been redirected from low-heat rejection engines toward increasing the durability of critical components [2]. Recently held international conferences and workshops devoted to the topic of the thermal barrier coatings (TBC) testify to the tremendous increase in the research and

* Corresponding author. Tel.: + 816-6879-8694; fax: + 816-6879-8689.

E-mail address: kobayasi@jwri.osaka-u.ac.jp (A. Kobayashi).

development of thermal sprayed coatings [3,4]. The R&D efforts highlight the fact that TBC behavior is not well understood and knowledge of the most fundamental problems, such as, failure mechanisms and durability are commonly at an empirical level.

Even more rudimentary is the progress in manufacturing and fundamental understanding of functionally graded coatings (FGC). The development of FGC using plasma spray techniques is still in an embryonic stage and will require significant R&D efforts [5]. The current work is aimed at enhancing the development of thermally sprayed FGC. To this end, a series of preparatory research activities were conducted to highlight the fundamental aspects of plasma spraying with mixed ceramic powders. The first activity centered on the production of high-density Ni-bonded WC coatings using various mixtures of fine Ni and WC powders [6]. Extremely high-density coatings were produced using a low power (5 kW) hollow-cathode plasma jet. The second set of experiments was conducted with mixtures of ZrO_2 and Al_2O_3 powders. The preliminary findings of this activity are described in this paper.

2. Experimental

A detailed description of the gas-tunnel-type plasma jet was given in Refs. [7–9]. Fig. 1 shows a schematic diagram of the gas-tunnel-type plasma jet, which consists of the “conventional” plasma jet and the vortex-stabilized plasma jet. During normal operation, the “conventional” plasma jet is turned off and only the vortex-stabilized section continues to operate. The conventional plasma torch is a hollow cathode type, which allows the injection of powders along the centerline of the gun. The powder then enters the vortex-stabilized plasma torch (vortex generator). This can be operated at a maximum power of 300 kW, however, for the current experiments the maximum power used was of the order of 20 kW.

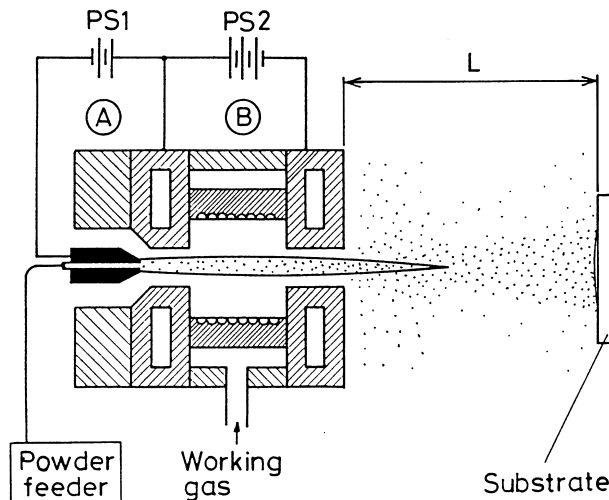


Fig. 1. Schematic diagram of gas-tunnel-type plasma torch: (A) conventional plasma torch, (B) vortex-stabilized plasma torch. PS-1, PS-2; power supplies.

Table 1
Operating conditions of gas-tunnel-type plasma jet

	Unit	Hollow cathode	Vortex generator
Power input	kW	5.3–6.5	20–30
Voltage unloaded/loaded	V	75/40	135/85
Cooling water flow rate	l/min	8	12
Working gas flow rate (Ar)	l/min	60	100–120
Powder carrier gas flow rate (Ar)	l/min	—	15–30
Spraying duration	s	—	5–30
Spraying distance	mm	—	50–70
Powder feed rate	g/min	—	7–18

All spraying tests were conducted inside a test chamber; however, the chamber was not evacuated and no shroud or filler gas was used. Argon was used as both the working gas for the plasma and as the carrier gas for the powder. The operating conditions of the gas-tunnel-type plasma jet (hollow-cathode DC plasma jet and the DC vortex generator) are shown in Table 1.

The test matrix consisted of spraying pure Al_2O_3 , 8% yttria-stabilized ZrO_2 , and three mixtures of ZrO_2 and Al_2O_3 . The wt% mixtures of the $\text{ZrO}_2/\text{Al}_2\text{O}_3$ were 80/20, 50/50, and 30/70. The powder size distribution of alumina and zirconia was between 20 and 40 μm . The substrate coupons were 3-mm-thick SUS-304 stainless steel, which were mechanically and chemically cleaned and then sandblasted. No bond coat was used between the substrate and the deposited coating. Results of the 50/50 wt% of $\text{ZrO}_2/\text{Al}_2\text{O}_3$ powder mixture are reported here.

Maximum coating thickness and footprint dimensions were recorded. The surface morphology of the coatings was photographed with a magnification of 200 before cutting the coated coupons. The coated coupons were then diamond-cut through their maximum thickness, and then padded using an extra low-viscosity resin. The samples were polished with a 0.25- μm diamond paste to a mirror-like finish. The optical microphotographs of the coating cross sections were taken at magnifications of up to 500 \times using a Leitz microscope. Vickers hardness measurements and X-ray diffraction (XRD) analysis were performed.

The morphology of the coatings is analyzed using the IMAGINETM Version 8.3 software¹. All image analyses were performed on the original microphotographs. However, to highlight the novel features of the composite coatings, a series of image enhancement procedures were conducted on the digitized optical microphotographs. Furthermore, for visualization purposes only, the morphology was plotted as a function of pixel intensity to generate a series of surface profile plots. This analysis allows a visual inspection of the microstructure of the composite coating. Porosity measurements and fractional percentages of composite constituents were carried out.

¹ ERDAS®, Inc. 2801 Buford Highway, Atlanta, GA, 30329-2137, USA.

3. Experimental results

3.1. Microphotographs

Fig. 2 shows a cross-sectional microphotograph of a coating made with a 50/50 wt%, $\text{ZrO}_2/\text{Al}_2\text{O}_3$ powder mixture before (Fig. 2a) and after image enhancement (Fig. 2b), which included removing of haze and sharpening. The purpose of the image enhancement is to highlight the unique microstructure features of the composite coating. As can be ascertained from Fig. 2, the microphotograph reveals three distinct areas: (1) black areas (pores), (2) gray areas (Al_2O_3), and (3) white areas (ZrO_2). In Fig. 2b, the morphology of the ZrO_2 clearly shows that the majority of the ZrO_2 is in the form of flat strips.

Fig. 3 depicts the sample used for Fig. 2 at a higher magnification ($500\times$). The advantage of simple image enhancement procedures becomes quite evident when Fig. 3a is compared with Fig. 3b. The structure of the ZrO_2 is now seen as splats embedded inside the Al_2O_3 matrix. Although Fig. 3b does not allow for clear distinction between pores and zirconia, the dark stripes in Fig. 3b are estimated to be zirconia. A tight bonding between the alumina and the zirconia is also expected from Figs. 3b and 2a (for example upper right corner).

3.2. Splat-morphology

The microphotograph depicted in Fig. 3 is indicative of a ceramic matrix composite structure, consisting of a large network of ZrO_2 splats inside a dense matrix of Al_2O_3 . The unique features of this composite coating structure are:

1. Alignment of ZrO_2 splats parallel to the substrate surface (\perp to spray direction).
2. Absence of porosity between the ZrO_2 splats and the Al_2O_3 matrix.
3. Relatively even distribution of ZrO_2 splats.
4. Fairly uniform thickness of ZrO_2 splats.
5. Good bonding between ZrO_2 splats and the Al_2O_3 matrix.

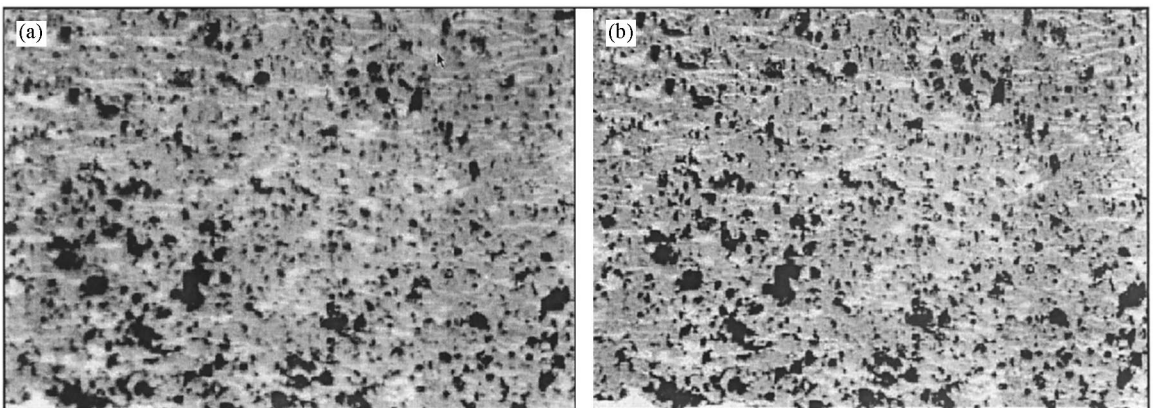


Fig. 2. Microphotograph of a coating produced with a 50/50 wt% $\text{ZrO}_2/\text{Al}_2\text{O}_3$ powder mixture: (a) raw data, (b) image enhanced ($200\times$ magnification).

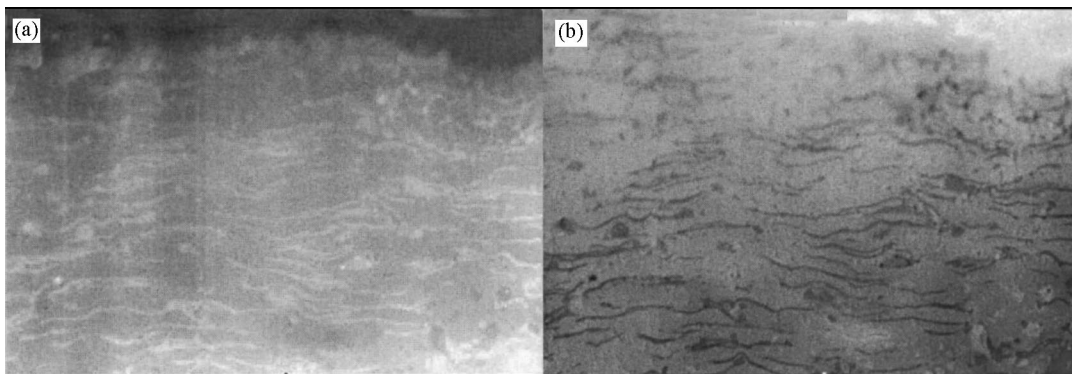


Fig. 3. Microphotograph of a coating produced with a 50/50 wt% $\text{ZrO}_2/\text{Al}_2\text{O}_3$ powder mixture: (a) raw data, (b) image enhanced ($500\times$ magnification).

3.3. Image analysis

All image analysis was conducted using the unaltered and raw microphotographs. Results of the analysis for the 50/50 wt% $\text{ZrO}_2/\text{Al}_2\text{O}_3$ composite coatings are given in Table 2. The most apparent result is lack of correlation between coating composition and that of the powder mixture weight ratios. The two oxides have vastly differing density, melting points, boiling points, and heat of formations as shown in Table 3. These properties influence all aspects of the coating process, from melting to solidification.

The difference in the density, the melting temperature, the heat of vaporization, and the heat of formation between the two ceramics indicates that the Al_2O_3 powder will undergo far more melting state inside the plasma flame. Thus, the fraction of molten Al_2O_3 splats reaching the substrates would be higher than that of the ZrO_2 under the same spraying conditions.

3.4. Surface profiling

The use of surface profiling software highlights the coating composition and morphology. Fig. 4 shows the surface profile along with cross-sectional profiles of the 50/50 wt% $\text{ZrO}_2/\text{Al}_2\text{O}_3$ coating. The area chosen for the analysis is outlined on the microphotograph adjacent to the surface profile.

The overall surface profile was generated as an image drape showing the entire microphotograph as shown in Fig. 4. The viewing direction is indicated on the microphotograph as “Eye” to “Target” arrow. Only large pores are discernable, while the zirconia is not clearly distinguishable from the alumina matrix. Image enhancement schemes are being investigated to improve such a morphology representation.

The unaltered original microphotograph was used for the profile analysis. The zirconia pixel intensity ranges between 198 and 230. The highest peaks depicted in Fig. 5 represent zirconia, while those ranging between 170 and 198 indicate zirconia. The deep “valleys” show the presence of pores. The cross-sectional profiles were picked perpendicular (side-A) and parallel (side-B) to the substrate surface. Side-A shows a series of sharp intensity peaks, which indicates a high degree of

Table 2
Image analysis results

Powder mixture	ZrO ₂ /Al ₂ O ₃
Mixing ratio (wt%)	50/50
Porosity (area%)	18.1
Al ₂ O ₃ (area%)	55.7
ZrO ₂ (area%)	26.2
ZrO ₂ /Al ₂ O ₃ (area ratio)	0.47

Table 3
Selected properties of Al₂O₃ and ZrO₂

Property	Unit	Al ₂ O ₃	ZrO ₂
Density	g/cm ³	3.97	5.89
Crystal structure		Hex	Cubic
Electrical resistivity (973 K)	Ω cm	5 × 10 ⁸	2300
Melting point	K	2322	3123
Boiling point	K	4173	4573
Thermal conductivity (298 K)	W/mK	27.21	3.04
Thermal expansivity	10 ⁻⁶ /K	5	10.1
Specific heat	kJ/mol at 298 K	419	460
Heat of fusion	J/g	1071	707

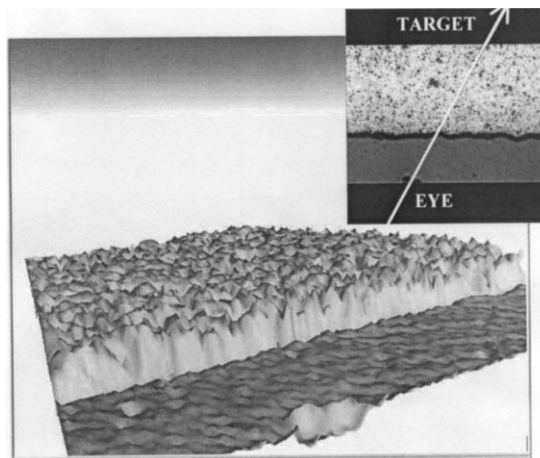


Fig. 4. An image drape of the 50/50 wt% ZrO₂/Al₂O₃ composite coating produced representing the surface morphology of the coating in terms of pixel intensity.

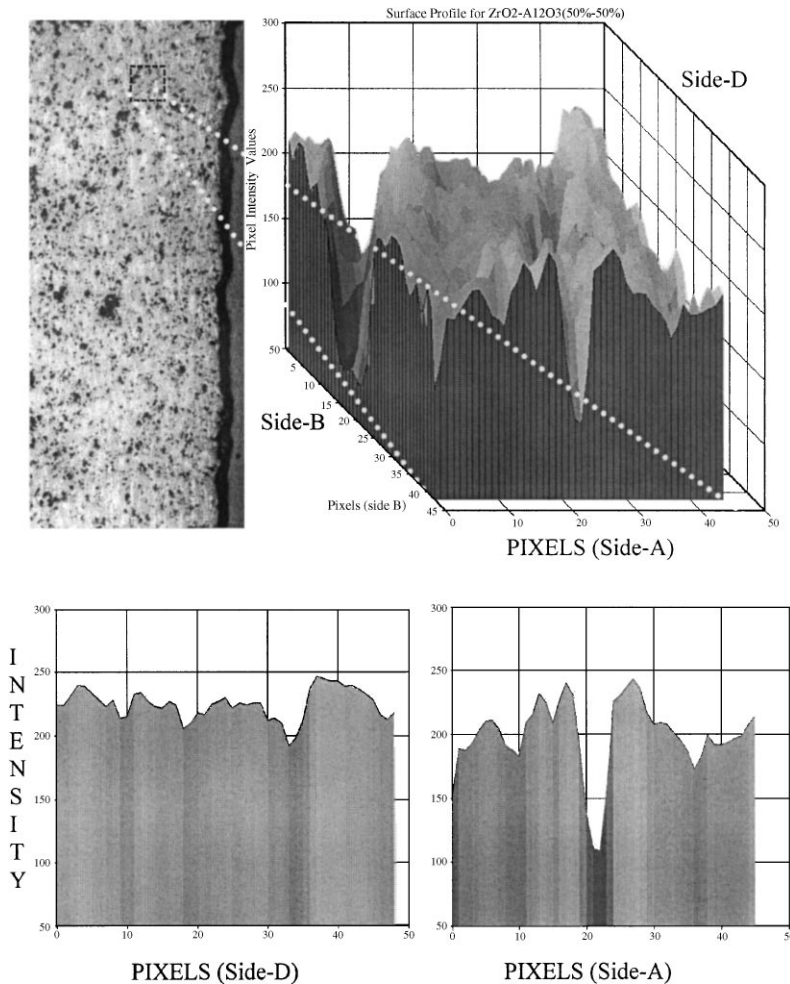


Fig. 5. Surface profile analysis of the 50/50 wt% ZrO_2/Al_2O_3 composite coating.

alternating ZrO_2 and Al_2O_3 material. In contrast to side-A, the profile depicted in side-D shows a large intensity across the plot. side-D thus coincides with the location of an ZrO_2 splat, which is aligned parallel to the substrate surface.

3.5. Discussion

Preliminary investigations of the 30/70 and the 80/20 wt% ZrO_2/Al_2O_3 powder mixture showed that the lowest porosity was found for coatings produced with the 50 wt% ratios. The higher melting temperature, higher specific heat, higher density, and lower thermal conductivity of the zirconia may result in a transfer of kinetic and thermal energy from the zirconia to the alumina during solidification. Therefore, different heating and solidification rates between the ZrO_2 and

Al_2O_3 are present. The solidification rate of alumina may be reduced in the presence of incoming molten ZrO_2 splats, because of transfer of thermal and kinetic energy from the zirconia to the alumina (ZrO_2 has higher heat capacity and has higher density). Because of the slower solidification rate, the alumina continues to flow along the surface of the already fully or partially solidified zirconia splats. The “flowing” alumina fills the crevices of the matrix, which results in a lower porosity for the composite. However, an analysis of the relative cooling rates of a mixture of different splat materials on a substrate needs to be performed before any definitive conclusions can be drawn.

4. Conclusion

Development of novel $\text{ZrO}_2\text{-Al}_2\text{O}_3$ thermal barrier composite coating was carried out by using the gas-tunnel-type plasma spraying. The best composite microstructure was found for a 50/50 wt% $\text{ZrO}_2\text{-Al}_2\text{O}_3$ powder mixture. A dense ceramic matrix composite coating with zirconia splats embedded inside a dense alumina matrix was formed. The unique composite microstructure showed the following features: (1) a relatively even distribution of embedded ZrO_2 splats in a Al_2O_3 matrix, (2) parallel alignment of the ZrO_2 splats relative to the substrate surface, (3) lack of porosity between the ZrO_2 splats and the Al_2O_3 matrix, (4) fairly uniform thickness of ZrO_2 splats, and (5) good bonding between the ZrO_2 splats and the Al_2O_3 matrix.

Because of the large difference in thermal conductivity between Al_2O_3 and ZrO_2 , 27 and 3 W/mK, respectively, this anisotropic composite coating should exhibit anisotropic thermal behavior. The higher conducting alumina matrix would facilitate heat conduction more readily parallel to the coating relative to the zirconia splats across the coating thickness.

Acknowledgements

The authors would like to acknowledge the financial support of the Ministry of Education, Science and Culture of Japan (Monbusho) and the School of Engineering and Applied Science at UCLA.

References

- [1] Brindley WJ et al., editors. Thermal Barrier Coating Workshop. Proceedings of a Conference, NASA Lewis Research Center, Cleveland, OH, March 27–29, 1995.
- [2] Yonushonis TM. Overview of thermal barrier coatings in diesel engines. *J Therm Spray Technol* 1997;6:50–6.
- [3] Narendra B et al., editors. Elevated temperature coatings: science and technology I. Proceedings of the Symposium on High Temperature Coatings I, TMS Fall Meeting, Rosemont, IL, October 3–6, 1994.
- [4] Thermal spray: a united forum for scientific and technological advances. Proceedings of the First United Thermal Spray Conference, Indianapolis, IN, September 15–18, 1997.
- [5] Berndt CC, editor. Composites and functionally graded materials. Proceedings of the Symposia, 1997 ASME International Mechanical Engineering Congress and Exposition, Dallas, TX, November 16–21, 1997.

- [6] Srivatsan TS et al., editors. Sharafat S, Kobayashi A, Chen S, Ghoniem NM. Production of high-density Ni-bonded tungsten carbide coatings using an axially fed DC-plasmatron, *Surface Coatings Technol*, April 2000 accepted for publication .
- [7] Arata Y, Kobayashi A, Habara Y, Jing S. Gas tunnel type plasma spraying apparatus. *Trans JWRI* 1986;15:227–31.
- [8] Arata Y, Kobayashi A, Habara Y. *J High Temp Soc* 1987;13:116–24.
- [9] Kobayashi A, Kurihara S, Habara Y, Arata Y. *J Weld Soc Jpn* 1990;8:457–63.